A New Approach to Modeling Vehicle-Induced Heat and Its Thermal Effects on Road Surface Temperature

AKIHIRO FUJIMOTO, AKIRA SAIDA, AND TERUYUKI FUKUHARA

Graduate School of Engineering, University of Fukui, Fukui, Japan

(Manuscript received 1 August 2011, in final form 17 May 2012)

ABSTRACT

The distribution of vehicle-induced wind velocity in the transversal direction of roads is measured. A statistical analysis is also performed to find the vehicle stopping time and stopping position at traffic signals. These results are used to build a heat-balance model to predict the road surface temperature resulting from the thermal effects of vehicles. To validate the model, measured and calculated road surface temperatures for a free-running (single path) location and a traffic-signal location are compared. The contributions of meteorological and vehicle-induced heat fluxes to the road surface temperature are quantitatively analyzed. For the present traffic and meteorological conditions, the calculated and measured road surface temperatures were in agreement for both the free-running and traffic-signal locations. Furthermore, the thermal contribution of vehicles to the road surface temperature was found to be nonnegligible at both locations.

1. Introduction

a. Background

The road surface temperature affects the safety of roads in winter and the thermal environment (such as heat islands) in urbanized areas. The heat-balance method used to predict the road surface temperature requires an accurate evaluation of the heat factors that influence the road surface. However, in contrast to the stochastic method, the heat-balance method does not require the correlations between the road surface temperature and natural factors (meteorology, topography, etc.) or artificial factors (traffic, salting, etc.) at specific points. The heat-balance method is, therefore, more versatile and adaptable than are statistical methods for the prediction of spatial variation in road surface temperatures. In particular, the thermal effects of traffic on road surface temperatures are usually nonnegligible in urban areas, while in mountainous and suburban areas, natural factors are more important. Surgue et al. (1983) reported that recorded road surface temperatures were usually several degrees Celsius higher in the road where traffic was heaviest. Gustavsson and Bogren (1991) showed road surface temperature differences of 1.5°C due to the differences in traffic conditions. Fujimoto et al. (2008) showed that the temperature in the vehicle-passage area, over which vehicles pass directly, was approximately 3°C lower than that in the non-vehicle-passage area, over which vehicles do not pass directly during a sunny winter day. Furthermore, Fujimoto et al. (2010) reported that the road surface temperature under vehicles waiting at traffic signals was 3°–4°C higher than that nearby.

These observations indicate that the thermal effects of vehicles on the road surface temperature are not negligible at traffic signals or when the volume of traffic is high.

b. Previous studies on thermal effects of vehicles and their modeling

Heat-balance models have been reported by Sass (1992), Shao and Lister (1996), Rayer (1987), Chapman et al. (2001), and Crevier and Yves (2001), among others. Unfortunately, these models did not include heat gain or loss through the road surface associated with passing vehicles. Recently, several researchers have modeled the thermal effects of vehicles on the road surface temperature. For example, by performing outdoor experiments, Ishikawa et al. (1999) built the first model incorporating longwave radiative heat from the bottom surface of the vehicle (hereafter referred to

Corresponding author address: Akihiro Fujimoto, Graduate School of Engineering, University of Fukui, 3-9-1 Bunkyo, Fukui City, Fukui 910-8507, Japan.
E-mail: afujimot@u-fukui.ac.jp

DOI: 10.1175/JAMC-D-11-0156.1

as the vehicle radiative heat). Prusa et al. (2002) showed the quasi-steady energy balance in the effective range of the vehicle-related heat (DM) surrounding a vehicle and evaluated the thermal fluxes generated by vehicles such as the surface thermal flux owing to frictional loss of a vehicle, radiant flux from a vehicle, sensible heat flux that occurs between the DM and the road surface, and so on. It is of interest that many heat fluxes in the energy balance equation in the DM are expressed using physical and thermodynamic laws. However, it is essential that we discuss whether the road surface temperature over the DM represents the temperature on the road surface in the vehicle-passage area and the relation between the vehicle-induced velocity and the eddy velocity that is the characteristic velocity of the largest eddies in the DM when using their model. Although Sato et al. (2004) indicated that the turbulent momentum transfer is enhanced by the eddy in the wake of a running vehicle, the effect of the turbulent momentum transfer on the road surface temperature was not reported quantitatively by analytical and experimental approaches. Watanabe et al. (2005) modeled the heat transmitted from the vehicle tires due to the friction between the tire and the road surface (hereinafter referred to as the tire frictional heat) and the shielding of solar radiation and sky radiation when the vehicle covers the road surface (hereinafter referred to as the vehicle's shield). Takahashi et al. (2006) proposed a heat-balance model considering the vehicle radiative heat and the vehicle's shield. The observed road surface temperatures for National Route 5 were compared with the calculated ones to find the accuracy of their model, but they did not show the increment or decrement of the road surface temperature due to the traffic conditions.

Subsequently, Fujimoto et al. (2008) developed a heat-transfer model by adding sensible heat due to the air movement by passing vehicles to the model built by Watanabe et al. These heat and air movements are hereafter referred to as the vehicle-induced sensible heat and vehicle-induced wind, respectively. We refer to this model as the vehicle road surface temperature (VRST) model. Fujimoto et al. (2008) also examined the thermal effects of vehicles on the road surface temperature by performing a numerical simulation using both an instantaneous and a time-averaged VRST model. The former calculates the time variation in vehicle-induced heat fluxes associated with the passage of vehicles (under pulselike conditions). The latter calculates the road surface temperature using time-averaged vehicle-induced heat fluxes. The following trends were observed: 1) the thermal effects of vehicles lowered the road surface temperature during the day and raised it at night and 2) the difference in the road surface temperatures of the two VRST models was small. Fujimoto et al. (2010) then conducted a simulation analysis of the road surface temperature at a traffic-signal location where vehicles repeatedly stop and start. The results showed that vehicles starting and stopping at traffic signals caused fluctuations in the road surface temperature, and that the temperature continuously fluctuated around 0°C (zero crossing).

Thus, the VRST model has made it possible to extract the properties of the road surface temperature overlooked in previous studies, by conducting experiments to identify heat transfer coefficients and variables relevant to traffic by field and indoor experiments using vehicles with tires. However, the VRST model has the following limitations:

1) Spatial changes in the vehicle-induced wind velocity are not considered (currently, the wind velocity at the center of the vehicle is used as a representative value).
2) At traffic-signal locations, it is assumed that vehicle stopping times and positions are fixed.
3) The VRST model has not been satisfactorily validated. A quantitative comparison of the calculated and observed road surface temperatures has not yet been performed at a traffic signal.

c. *Purpose of study*

This study had the following major objectives:

1) to derive a rational relationship between the vehicle speed and vehicle-induced wind velocity on the basis of the distribution of vehicle-induced wind velocity in the transversal direction of the road,
2) to elucidate the properties of vehicle stopping time and position at traffic signals,
3) to improve the vehicle-induced sensible heat and vehicle radiative heat using the results obtained from objectives 1 and 2, and
4) to verify the reliability of the improved VRST model by comparing observed and calculated road surface temperatures at a free-running (single path) location and a traffic-signal location.

2. VRST model

a. *Assumptions*

The VRST model is based on several assumptions. For vehicle operation, there are three assumptions:

1) The target road surface is the center of the lane (i.e., at the vehicle's centerline). At traffic-signal locations,

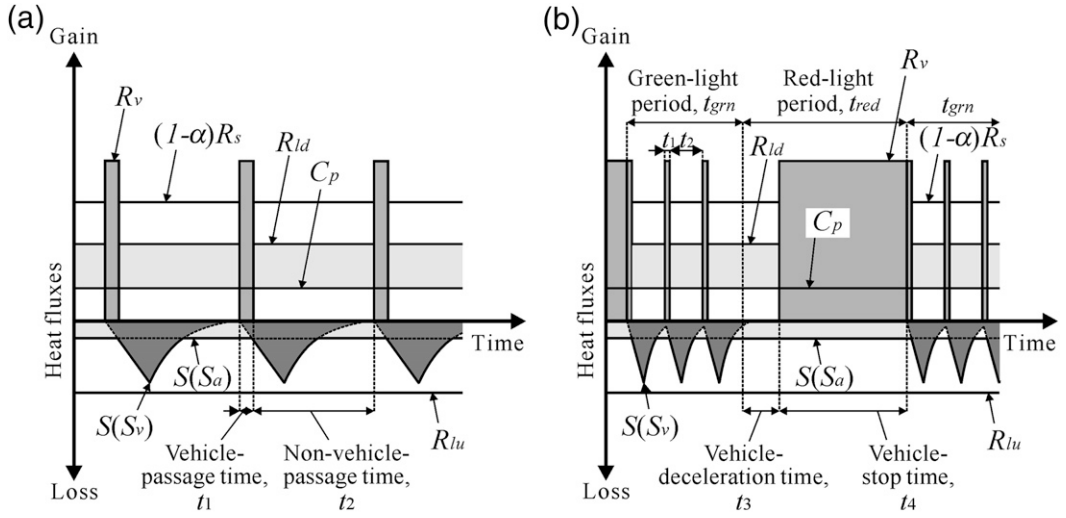

FIG. 1. Time variations in heat fluxes due to passing of vehicles, shown for (a) a free-running location and (b) a traffic-signal location.

the center of the vehicle that is stopped just before the stop line is the target road surface.

2) All vehicles travel in the center of the lane and are the same size.
3) The time interval between any two vehicles (the vehicle-passage time) is uniformly distributed on the basis of the hourly traffic volume.

For heat flux, there are two additional assumptions:

4) Heat transfer in the transversal direction of the road is neglected.
5) Additional wind velocity due to the interactions between natural wind and vehicle-induced wind is not considered. That is, there is no superposition of these two winds, and the sensible heat associated with a relatively high wind velocity is incorporated in the heat balance of the pavement surface layer [Eq. (1)].

b. Heat balance on pavement surface

The spikelike changes in heat flux in response to the passing of vehicles are expressed using unit step functions whose values are 0 or 1 [$f(t)$ and $g(t)$], and the heat balance of the pavement surface layer is given by

$$\rho_p c_p \frac{\partial T_p}{\partial t}\Delta z_s = C_p - R_{\mathrm{lu}} + S + L + f(t)[R_{\mathrm{ld}} + (1-\alpha)R_s] + g(t)R_v = Q_{\mathrm{net}}, \quad (1)$$

where ρ_p is the density of the pavement surface layer (kg m^{-3}), c_p is the specific heat of the pavement surface (kJ kg^{-1} K^{-1}), T_p is the temperature of the pavement surface layer (°C), t is the time (s), Δz_s is the thickness of the pavement surface layer (m), C_p is the pavement conductive heat flux (W m^{-2}), R_{lu} is the road surface radiative heat flux (W m^{-2}), S is the sensible heat flux (W m^{-2}), L is the latent heat flux (W m^{-2}), R_{ld} is the sky radiative heat flux (W m^{-2}), α is the albedo, R_s is the shortwave (insolation) heat flux (W m^{-2}), R_v is the vehicle radiative heat flux (W m^{-2}), and Q_{net} is the net heat flux (W m^{-2}). Here, S is given by the following formula based on assumption 5 in section 2a:

$$S = \begin{cases} S_a & \text{for} \quad V_{\mathrm{nw}} \geq V_w \\ S_v & \text{for} \quad V_{\mathrm{nw}} < V_w \end{cases}, \quad (2)$$

where V_{nw} is the natural (background) wind velocity (m s^{-1}), S_a is the natural wind sensible heat flux arising from V_{nw} (W m^{-2}), V_w is the vehicle-induced wind velocity (m s^{-1}), and S_v is the vehicle-induced sensible heat flux arising from V_w (W m^{-2}). The details of the heat flux in Eqs. (1) and (2) have been described by Fujimoto et al. (2008), and no further explanation is given here. In addition, in this analysis, the road surface is considered to be dry, and, therefore, L is eliminated. The unit step functions in Eq. (1) will be discussed in detail in the next section.

c. Modeling thermal effects of vehicles

Figures 1a and 1b show the time variations in the heat fluxes due to the passing of vehicles at free-running and traffic-signal locations, respectively.

1) FREE-RUNNING LOCATION

In Fig. 1a, t_1 is the period during which the road surface is covered by a moving vehicle (the vehicle-passage time), and t_2 is the subsequent period during which it is

TABLE 1. Unit step function for heat balance on road surface.

Period	$f(t)$	$g(t)$	Subject road surface
t_1	0	1	Free-running location
t_2	1	0	
t_3	1	0	Traffic-signal location
t_4	0	1	

not covered (the non-vehicle-passage time). The quantities C_p, R_{lu}, and S act on the road surface at all times. During t_1, R_v acts on the road surface while R_{ld} and R_s are zero. Conversely, during t_2, R_{ld} and $(1-\alpha)R_s$ act on the road surface while R_v is zero. The values of t_1 and t_2 are defined by the following equations:

$$t_1 = \frac{L_v}{V_v} \times 1000 \quad \text{and} \tag{3}$$

$$t_2 = \frac{1}{F_v} - t_1, \tag{4}$$

where L_v is the vehicle length (m), V_v is the vehicle speed (km h^{-1}), and F_v is the hourly traffic volume (vehicles per hour).

2) TRAFFIC-SIGNAL LOCATION

In this section, we consider the time taken for a vehicle to stop at the designated point (just before the stop line) after the traffic signal turns red (i.e., the vehicle deceleration time), and the period for which the vehicle remains stationary until the next green signal (vehicle stop time). The stop time at the designated point, t_4, is given by

$$t_4 = t_{red} P_{st} P_{sa}, \tag{5}$$

where t_{red} is the red-signal period that includes the yellow-signal period, P_{st} $(=t_{40}/t_{red})$ is the stop-time ratio, and P_{sa} $(=N_s/N_{s0})$ is the stopping-vehicle-number ratio. In addition, t_{40} is the stop time corresponding to the red-signal period (s), N_{s0} is the frequency of the red signal per unit time, and N_s is the frequency of the red signal when a vehicle stops at the designated point in N_{s0}; t_{40} is the mean of the stop times measured at a traffic signal. As will be discussed in section 4b, N_s and t_{40} may be affected by the traffic volume.

Finally, from Eq. (5), the vehicle deceleration time, t_3 (h), is

$$t_3 = t_{red} - t_4. \tag{6}$$

Given the above thermal effects of vehicles, the unit step functions $f(t)$ and $g(t)$ in Eq. (1) are as listed in Table 1.

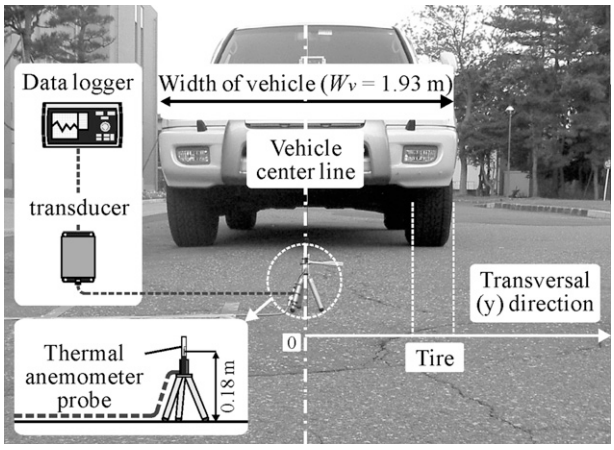

FIG. 2. Outline of vehicle-induced wind-velocity measurements.

3. Measurement and formulation of vehicle-induced wind velocity

a. Outline of experiment

To study the distribution of V_w in the transversal y direction of the road, we conducted an outdoor experiment using a typical passenger vehicle (4.97 m in length, 1.93 m in width, and 1.86 m in height). A thermal anemometer (manufactured by Kanomax) was set up at a height of 0.18 m above the road surface as shown in Fig. 2, and the y direction of V_w was measured by translating the driving of the vehicle in the y direction.

The vehicle's centerline was considered to be $y = 0$. The vehicle's speed was set to 30 km h^{-1}.

b. Transversal distribution of vehicle-induced wind velocity

Figure 3 shows the time variations in V_w for $y^* = 0$, 0.4, 1.2, and 1.6, where y^* is the normalized distance and $y^* = y/0.5W_v$ (W_v being the vehicle width). The value

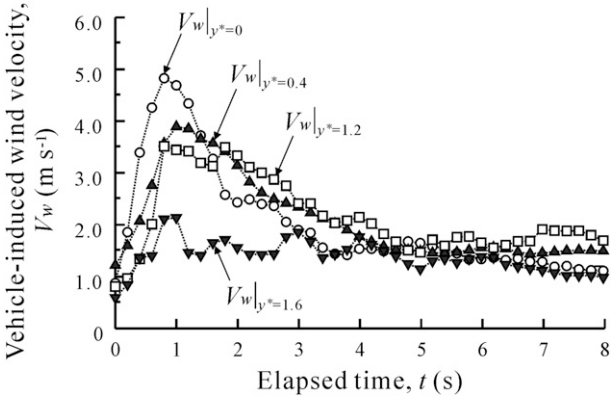

FIG. 3. Time variations in vehicle-induced wind velocity V_w at normalized distance y^*.

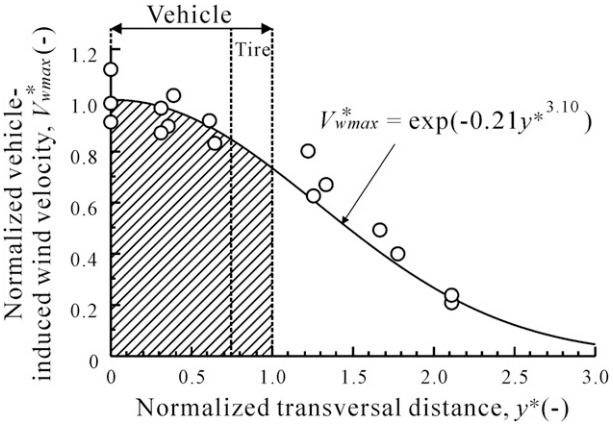

FIG. 4. Relationship between maximum normalized vehicle-induced wind velocity $V^*_{w\max}$ and normalized distance y^*.

of V_w increases rapidly immediately after the vehicle passes ($t = 0$), reaching a peak at approximately 1 s and then decreasing gradually.

The maximum value of V_w, $V_{w\max}$ (m s^{-1}), occurred at the center of the vehicle (i.e., $y^* = 0$) and decreased toward the roadside (as y^* became larger). We have normalized $V_{w\max}$ to express the y direction of V_w in a unified expression:

$$V^*_{w\max} = \frac{V_{w\max} - V_{\mathrm{nw}}}{V_{w\max 0} - V_{\mathrm{nw}}}, \tag{7}$$

where $V_{w\max 0} = V_{w\max}|_{y^*=0}$ and $V^*_{w\max} = 0$ indicates that $V_{w\max} = V_{\mathrm{nw}}$.

Figure 4 shows the relationship between $V^*_{w\max}$ and y^*. Here, $V^*_{w\max}$ decreases as y^* increases, and the relationship between $V^*_{w\max}$ and y^* follows a Gaussian function. That is,

$$V^*_{w\max} = \exp(-0.31y^{*2.10}). \tag{8}$$

c. Representative velocity of vehicle-induced wind

In determining the representative value of V_w, $\overline{V_w}$, the following assumptions were made:

1) Time variations in $V_w|_{y^*=0}$ ($=V_{w0}$) depend on t but do not depend on y^*, as shown in Eq. (9), established by Fujimoto et al. (2008):

$$V_{\mathrm{w0}} \begin{cases} = at & (0 \le t \le t_{\max}) \\ = V_{w\max 0} \exp[-b(t - t_{\max})] - c(t - t_{\max}) & (t_{\max} \le t \le t_0) \end{cases}, \tag{9}$$

where $t_{\max}$ is the time (s) for the wind velocity to reach $V_{w\max 0}$ from the ambient velocity, t_0 is the duration of the vehicle-induced wind, and a, b, and c are coefficients. For vehicle speeds V_v (km h^{-1}) ranging from 10 to 70 km h^{-1}, these variables and coefficients are formulated in terms of V_v as follows (see Fujimoto et al. 2008):

$$a = 0.08V_v, \tag{10}$$

$$b = 0.28 \times 10^{-2}V_v + 0.13, \tag{11}$$

$$c = V_{w\max 0} \exp[-b(t_0 - t_{\max})]/(t_0 - t_{\max}), \tag{12}$$

$$V_{w\max 0} = 0.08V_v, \tag{13}$$

$$t_{\max} = 1.2 \exp(-0.3 \times 10^{-2}V_v), \quad \text{and} \tag{14}$$

$$t_v = -1.4 \times 10^{-2}V_v + 7.6. \tag{15}$$

In addition, t in Eq. (9) indicates the elapsed time (s) since the vehicle passage.

2) The representative value of $V^*_{w\max}$, $\overline{V^*_{w\max}}$, is the average of $V^*_{w\max}$ over half of the vehicle width (from $y^* = 0$ to 1.0, the shaded area in Fig. 4).

3) Here, $\overline{V_w}$ is the product of V_{w0} and $\overline{V^*_{w\max}}$. On the basis of these assumptions and Eq. (8), $\overline{V_w}$ is calculated as follows:

$$\overline{V_w} = V_{\mathrm{w0}}\overline{V^*_{w\max}}, \tag{16}$$

where

$$\overline{V^*_{w\max}} = \int_0^{1.0} V^*_{w\max}\, dy^* = 0.91. \tag{17}$$

4. Micrometeorological observation, traffic-volume survey, and road surface temperature measurement on a national route

a. Outline of observation

This section describes the micrometeorological observations, the traffic-volume survey, and the road surface temperature measurements (hereinafter referred to as the observations). The observations were made at the free-running location and the traffic-signal location, and these are labeled case BS and case CS, respectively.

Case BS was measured at National Route 8 (Echizen City, Fukui, Japan) from 0700 to 1700 LT 6 August 2008. Case CS was measured at an intersection on National Route 416 (Fukui City, Fukui) from 1700 to 0800 LT 29–30 December 2009. In both observations, the air temperature T_a and the relative humidity RH_a (%) were measured using a thermohygrometer (HMP45, manufactured by Vaisala). The value of V_{nw} (m s^{-1}) was measured using a vane anemometer (Weather Wizard III, manufactured by Davis). Both R_s and R_{ld} were measured using a radiation balance meter (CNR1, manufactured by Kipp and Zonen). These values were recorded every minute by a datalogger. The road surface temperature T_s was measured using a radiation thermometer (ST 60, manufactured by Raytek) at points within and outside the vehicle's passage. Furthermore, the spatial distribution of the road surface temperature was regularly recorded using a thermotracer (TH9100, manufactured by NEC). In case BS, V_v was calculated by measuring the traveling time between two different positions. In case CS, the green-light period t_{grn}, t_{red}, t_4, and the vehicle-stopping positions near the traffic signal were recorded using a video camera.

b. Observation results

Figures 5 and 6 show the time variations in T_a, RH_a, V_{nw}, R_s, R_{ld}, and F_v for cases BS and CS, V_v for case BS only, and t_{grn}, t_{red}, and t_4 for case CS only.

1) FREE-RUNNING LOCATION

The weather on the day of observation was fine until 1200 LT, and then it became cloudy. The road surface was completely dry all day. The value of T_a increased from 23.1°C at 0700 LT to 34.8°C at 1230 LT, which was the maximum temperature during the observation period. Subsequently, T_a was around 30°C until 1700 LT. The value of RH_a decreased from approximately 80% at 0700 LT to approximately 40% at 1000 LT. Subsequently, RH_a varied within a range of 40%–60%, while V_{nw} was below 1 m s^{-1} until 1200 LT and reached a maximum of 2.4 m s^{-1} at 1300 LT. Subsequently, V_{nw} was in the range 0.5–2.0 m s^{-1}, and R_s increased from the beginning of the observation to a maximum of 908 W m^{-2} at 1200 LT. It then oscillated because of the effect of the clouds. The value of R_{ld} ranged from 420 to 475 W m^{-2}, while F_v ranged from 270 to 500 vehicles per hour with an average value of 376 vehicles per hour. In addition, V_v varied between 37 and 42 km h^{-1} with an average value of 38 km h^{-1}.

2) TRAFFIC-SIGNAL LOCATION

During the observation period, the weather was fine and the road surface was dry. The value of T_a decreased from 5.7°C at the beginning of the observation to 1.0°C at 0000 LT and then increased to around 2.0°C, while RH_a was 60%–70% throughout the observation period. For most of the time, V_{nw} was less than 0.4 m s^{-1}, and the maximum V_{nw} of 0.7 m s^{-1} was reached at 0100 LT. The value of R_{ld} was approximately 300 W m^{-2}, while F_v decreased from approximately 360 vehicles per hour from 1700 to 1900 LT to a minimum of 51 vehicles per

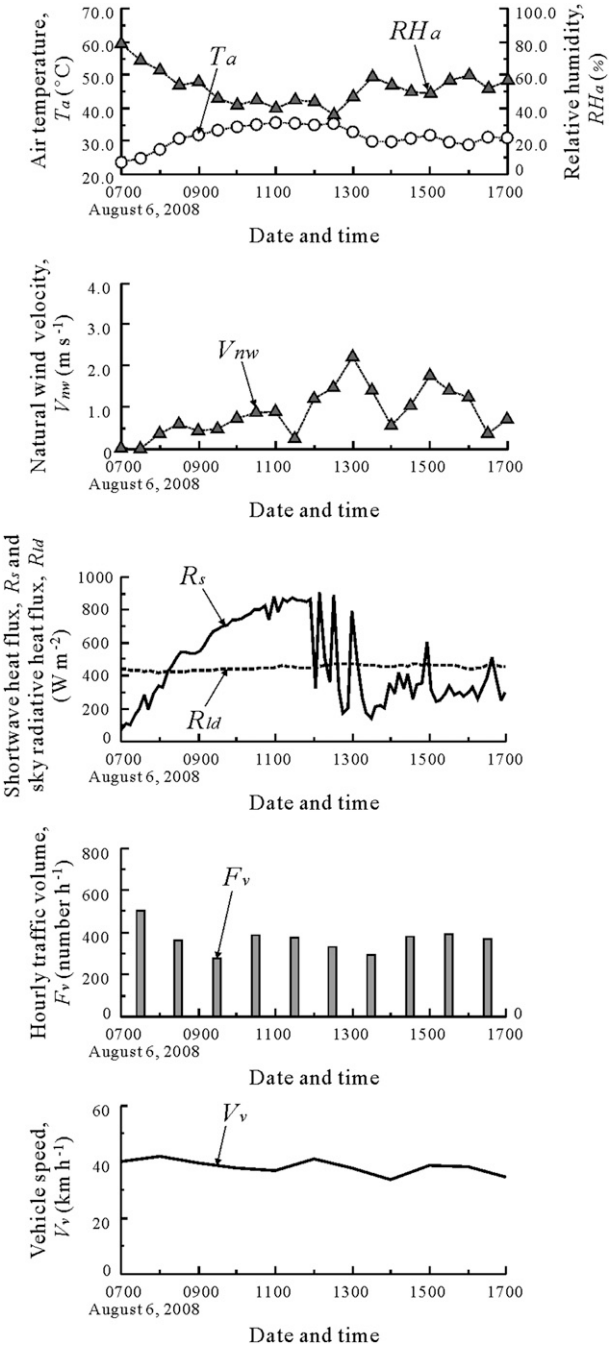

FIG. 5. Observation results (free-running location).

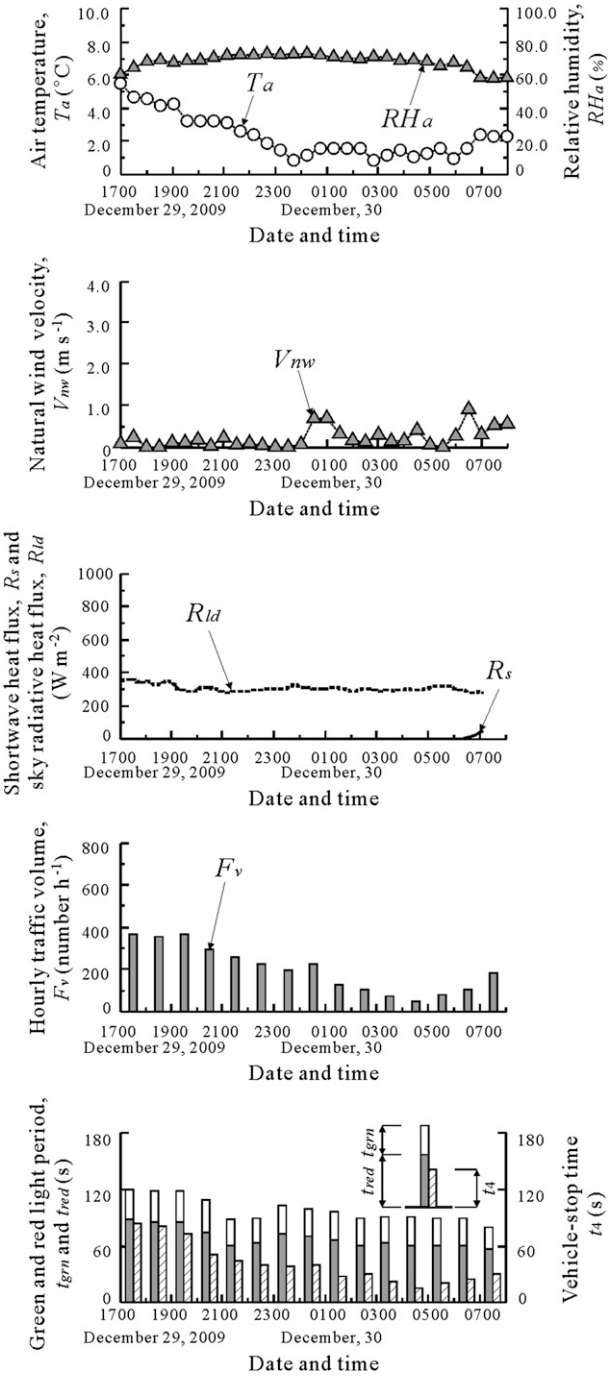

FIG. 6. Observation results (traffic-signal location).

hour at 0400 LT. Throughout the observation period, t_{grn} was approximately 30 s, while t_{red} was approximately 90 s from 1700 to 2000 LT and ranged from 60 to 75 s for the rest of the observation period. Furthermore, t_4 was almost equal to t_{red} at 1700 and 1800 LT but became shorter as F_v decreased, reaching a minimum of 16 s at 0400 LT.

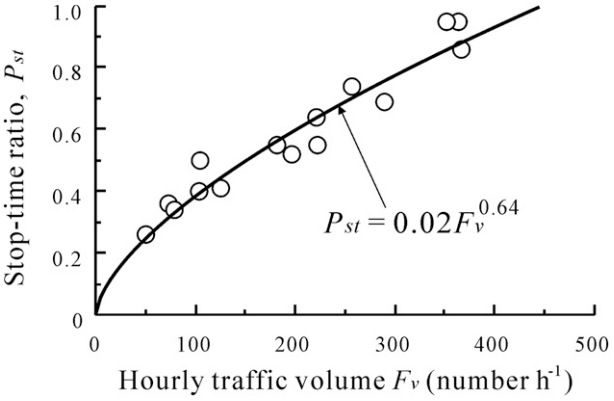

FIG. 7. Relationship between stop-time ratio P_{st} and hourly traffic volume F_v.

Figures 7 and 8 show the relationship between P_{st} or P_{sa} and F_v. The value of P_{st} increased in proportion to the power function of F_v and is given by

$$P_{st} = 0.02F_v^{0.64}. \quad (18)$$

The relationship between P_{sa} and F_v is given by the same type of function as that for the relationship between P_{st} and F_v:

$$P_{sa} = 0.30F_v^{0.18}. \quad (19)$$

5. Comparison of measured and calculated results of road surface temperature

a. Boundary conditions and initial conditions

A numerical analysis of the road surface temperature was performed for a pavement body of thickness 0.5 m

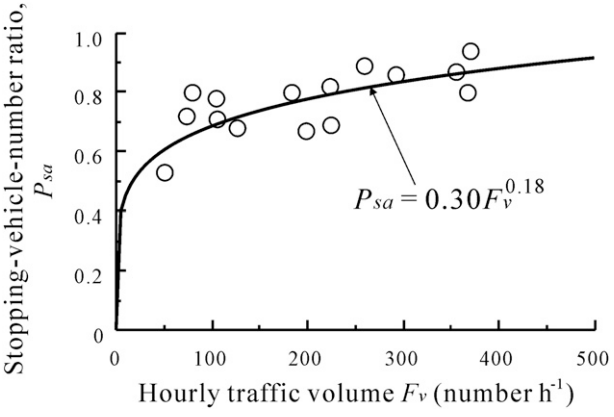

FIG. 8. Relationship between stopping-vehicle-number ratio P_{sa} and hourly traffic volume F_v.

TABLE 2. Thermophysical property values for pavement and ground.

Layer	Depth (thickness, m)	Density (kg m^{-3})	Specific heat (J g^{-1} K^{-1})	Thermal conductivity (W m^{-1} K^{-1})
Asphalt layer	0–0.1 (0.1)	2.3	0.9	1.6
Subgrade	0.1–0.5 (0.4)	2.0	1.0	1.8
Ground	0.5–5.4 (4.9)	2.0	1.6	1.6

and a subgrade of thickness 4.9 m. To obtain the initial temperatures in the pavement and subgrade, we entered weather data for August and December (from Fukui Local Meteorological Observatory) into the model and carried out a transient analysis until the vertical temperature profile varied with the thermal equilibrium state. The weather and traffic data obtained from the observations were used as the boundary conditions and were given by a linear interpolation of the data collected in time order. The temperature of the bottom boundary of the analysis area was fixed at 15°C in case BS and 10°C in case CS. In addition, on the basis of assumption 4 in section 2, it was considered that there was no heat transfer at the side boundary of the analysis area. Since V_v could not be measured in case CS, it was fixed to 32 km h^{-1} with reference to the Fiscal 2005 Road Traffic Census. Table 2 lists the thermophysical property values given in a heat-transfer handbook (written by the Japan Society of Mechanical Engineers in 1993, pp. 238 and 375) for the pavement and ground used in the analysis.

b. Spatial distribution and time variation of road surface temperature

The model was validated by comparing the observed T_s with the calculated T_s. We also discuss the difference in T_s between the vehicle-passage and non-vehicle-passage areas.

1) FREE-RUNNING LOCATION

Figures 9a and 9b show the spatial distribution of T_s in case BS at 0635 and 1157 LT 6 August 2008. In Fig. 9a we see that T_s at all points (A–F) was almost uniform, in the range 27.2°–27.8°C, whether or not vehicles were passing. However, the values of T_s at points G, J, I, and L in the vehicle-passage area in Fig. 9b (50.6°–53.6°C) were approximately 1°–3°C lower than T_s at points H and K without vehicle passage (54.4°–54.8°C).

Figure 10 shows the time variation in T_s in case BS. Hereinafter, the suffixes v and n for T_s indicate the vehicle- and non-vehicle-passage areas, respectively, and the suffixes m and c indicate the measured and calculated values, respectively.

The initial T_{svm} and T_{snm} were both 30.6°C, and there was no difference between them: ΔT_{sm} ($= T_{svm} - T_{snm}$) = 0. Both T_{svm} and T_{snm} increased over time, but T_{snm} became higher than T_{svm} at around 0900 LT. Both values reached a maximum at 1200 LT (T_{snm} = 55.5°C and T_{svm} = 51.2°C) with $\Delta T_{sm} = -4.3$°C. Subsequently, both temperatures decreased gradually while maintaining $\Delta T_{sm} \approx -1.5$°C. The average ΔT_{sm} during the observation period $\overline{\Delta T_{sm}}$ was −2.0°C.

The calculated temperatures, T_{svc} and T_{snc}, reproduced the observed values in general, as shown in Fig. 10. However, when the vehicle-induced sensible heat S_v is deleted from the heat balance in Eq. (1) [i.e., $S = S_a$ in Eq. (1)], the calculated road surface temperature T'_{svc} was slightly lower than T_{snc} and became more inaccurate than T_{svc}. As far as the present traffic and meteorological conditions are concerned, it is seen that S_v cannot be disregarded from the calculation of the road surface temperature.

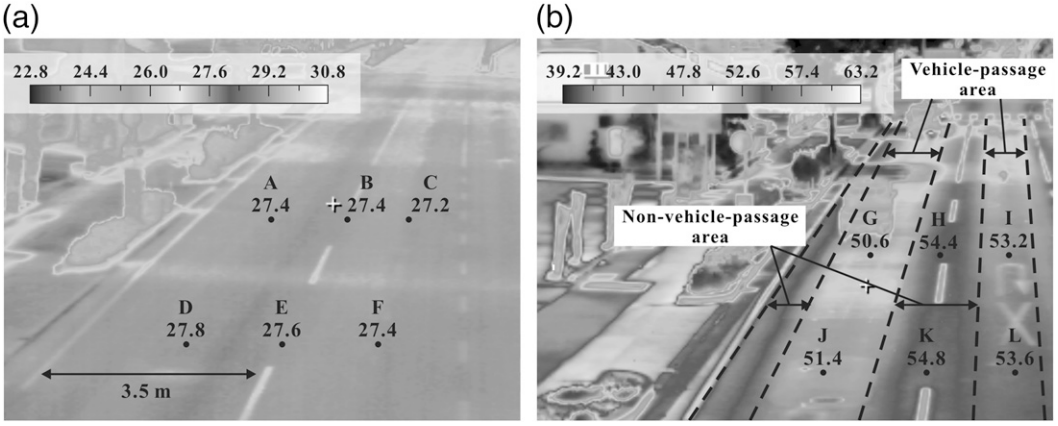

FIG. 9. Spatial distribution of road surface temperature (free-running location) at (a) 0635 and (b) 1157 LT 6 Aug 2008.

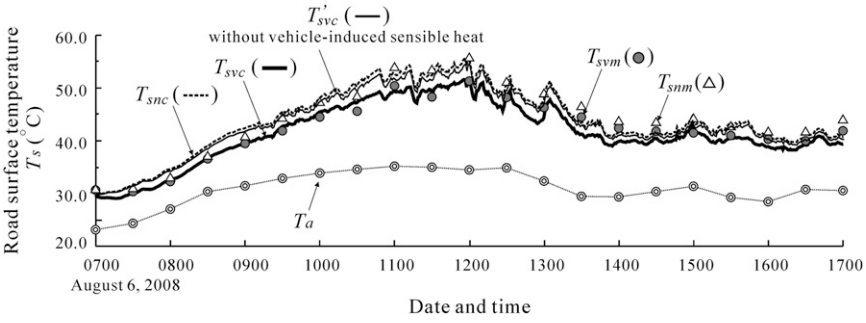

FIG. 10. Time variation in road surface temperature T_s (free-running location).

During the observation period, the average difference between T_{svc} and T_{snc}, ΔT_{sc} ($=T_{svc} - T_{snc}$), was −2.0°C, which was in good agreement with $\overline{\Delta T_{sm}}$.

2) TRAFFIC-SIGNAL LOCATION

Figures 11a and 11b indicate the spatial distribution of T_s in case CS at 2102 and 2103 LT 29 December 2009. It is evident from Fig. 11a that the vehicle-body temperature is higher than T_s except on the roof, side-view mirrors, and so on. The values of T_s at points M, N, and O in the non-vehicle-passage area were 7.2°, 8.6°, and 9.5°C, respectively. Here, T_s increased as the measurement point was closer to the vehicle-passage area. In Fig. 11a, the values of T_s at points P, S, R, and U in the vehicle-stopping area were 3°–4°C higher than T_s at points Q and T in the zone where vehicles did not stop or did not pass.

According to Prusa et al. (2002), the width of the DM is 1.7–3.9 times that of a vehicle. Consequently, it is clear from Fig. 11 that the road surface temperature over the DM is not uniform. There is an obvious difference in the road surface temperature between the vehicle-passage area and the non-vehicle-passage area. The road surface temperature in the vehicle-passage area can be regarded as the representative surface temperature on the road that is subject to the vehicle-related heat.

Figure 12 shows the time variations in T_s in case CS. At the beginning of the observation T_{svm} and T_{snm} were 10.9° and 8.2°C, respectively. Slight fluctuations in the temperature continued throughout the observation period. At the beginning of the observation, ΔT_{sm} was 2.7°C, reaching 4.9°C at 2000 LT and then decreasing over time. After 0100 LT, ΔT_{sm} was approximately 0.5°C and the value of $\overline{\Delta T_{sm}}$ was 1.9°C.

While T_{snc} varied gradually over time, T_{svc} showed fluctuations with a small amplitude. The top-right graph in Fig. 12 shows an enlarged view of the time variation in T_{svc} (solid line). It is evident that T_{svc} decreased for t_{grn} (shown as A) and increased for t_{red} (shown as B and C). The cause of the fluctuation will be discussed in detail in section 6a(2).

The amplitude for T_{svc}, ΔT_{svc}, was approximately 0.3°C for F_v = 360 vehicles per hour at 1700–1900 LT, approximately 0.2°C for F_v = 225 vehicles per hour at 0000 LT, and lower than 0.1°C for F_v = 51 vehicles per hour at 0400 LT. Increases in F_v tended to increase ΔT_{svc}.

The values of T_{snc} and T_{svc} were in good agreement with the measured temperatures, T_{snm} and T_{svm}. In addition, $\overline{\Delta T_{sc}}$ was 1.6°C, which was 0.3°C lower than $\overline{\Delta T_{sm}}$.

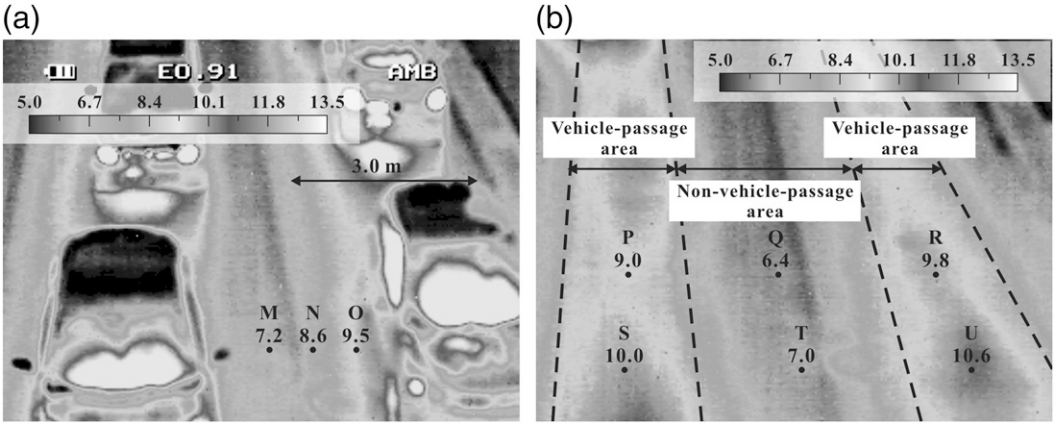

FIG. 11. Spatial distribution of road surface temperature (traffic-signal location) at (a) 2102 and (b) 2103 LT 29 Dec 2009.

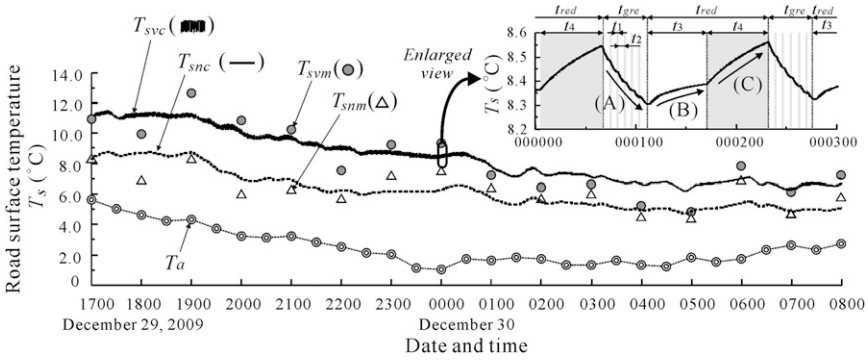

FIG. 12. Time variation in road surface temperature T_s (traffic-signal location).

This difference between $\overline{\Delta T_{sc}}$ and $\overline{\Delta T_{sm}}$ may depend on the temperature measurement position on the road surface and may be caused by an error in the initial temperature of the pavement body or subgrade.

6. Discussion

a. Heat balance on road surface

1) FREE-RUNNING LOCATION

Figures 13a and 13b show the time variation in heat flux in the non-vehicle-passage area from 0700 to 1700 LT 6 August 2008 and in the vehicle-passage area for 20 s from 1105:30 to 1105:50 LT 8 August 2008 in case BS. The positive vertical (y) axis (top half) and the negative y axis (bottom half) indicate the heat gain and loss, respectively, of the road surface layer.

We first discuss the heat flux in the non-vehicle-passage area in Fig. 13a. The main causes of heat gain were $(1-\alpha)R_s$ and R_{ld}, while R_{lu} and C_p before 1300 LT and R_{lu} and $S = S_a$ after 1300 LT were the main causes of heat loss. The values of R_{lu} and C_p were almost constant at approximately -573 and -339 W m^{-2}.

We now consider the heat flux in the vehicle-passage area in Fig. 13b. For the t_1 period (0.4 s), $(1-\alpha)R_s$ and R_{ld} were zero because of the vehicle's shielding effect, but were 645 and 451 W m^{-2}, respectively, for the t_2 period (9.1 s). Instead, an R_v of 547 W m^{-2} acted on the road surface for the t_1 period. The maximum value of S_a was -136 W m^{-2} when $V_{nw} > V_w$, and the maximum value of S_v reached -409 W m^{-2} (=3 times larger than S_a) when $V_{nw} < V_w$. It is seen that S_v contributes to the decrease in the road surface temperature shown in Fig. 10 (i.e., $T_{svc} < T'_{svc}$), and that a running vehicle plays the role of a fan that cools the road surface.

2) TRAFFIC-SIGNAL LOCATION

Figures 14a and 14b show the time variations in the heat flux in the non-vehicle-passage area from 1700 to 0800 LT 29 December 2009 and in the vehicle-passage area for 3 min from 0000 LT 30 December 2009 in case CS.

In the non-vehicle-passage area in Fig. 14a, the heat loss by R_{lu} and heat gain by R_{ld} were dominant, and $S = S_a$, C_p, and $(1-\alpha)R_s$ were relatively small.

We now discuss the heat flux in the vehicle-passage area in Fig. 14b. The values for t_1, t_2, t_3, and t_4 during this period were 0.5, 4.1, 34.3, and 35.9 s, respectively. For the t_2 and t_3 periods, R_{ld} was 319 W m^{-2} and reached zero for the t_1 and t_4 periods. For the t_1 and t_4 periods R_v, was 369 W m^{-2}. The maximum value of S_a was

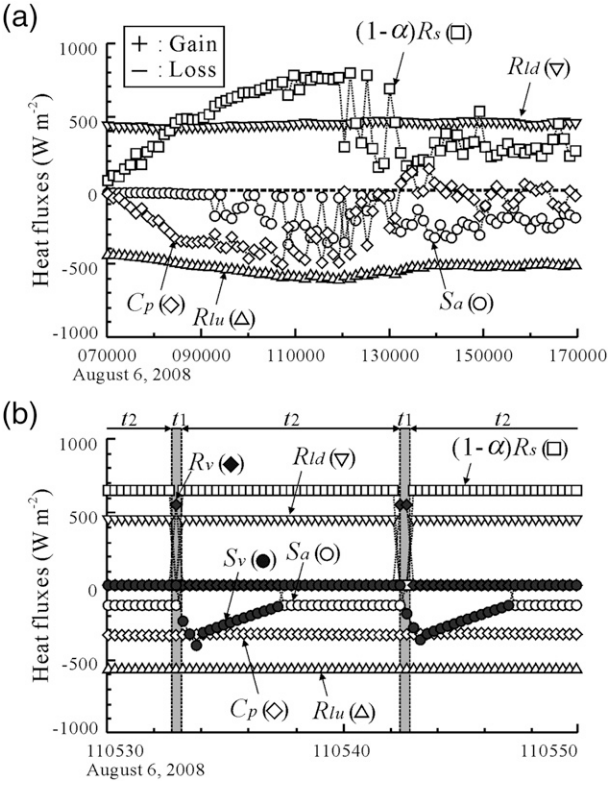

FIG. 13. Time variation in heat fluxes (free-running location) at (a) a non-vehicle-passage area and (b) a vehicle-passage area.

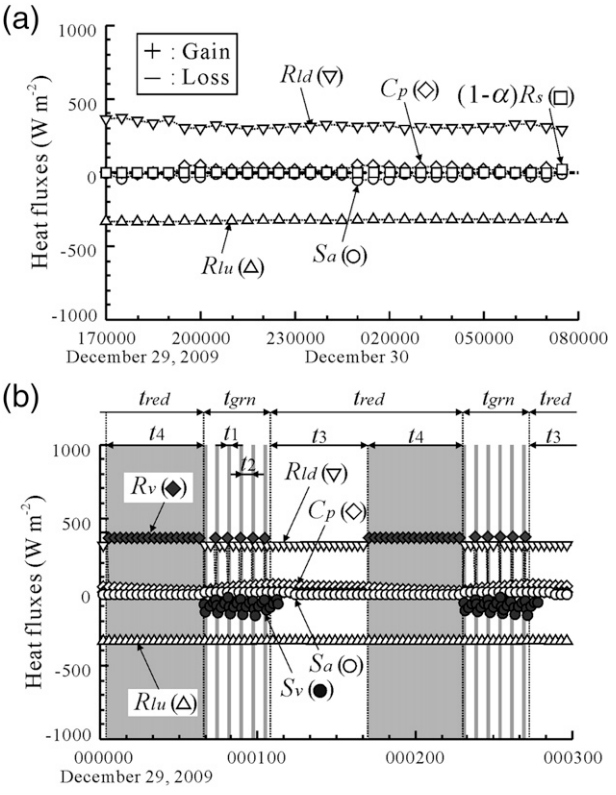

FIG. 14. Time variation in heat fluxes (traffic-signal location) at (a) a non-vehicle-passage area and (b) a vehicle-passage area.

-16 W m^{-2} when $V_{nw} > V_w$, and S_v reached a maximum value of -164 W m^{-2} when $V_{nw} < V_w$. Here, C_p increased as if to compensate for the negative S_v for t_{grn} and reached a maximum value of 54 W m^{-2}, but decreased for t_{red}. The value of R_{lu} was -332 W m^{-2}.

The average Q_{net} values for the t_1, t_2, t_3, and t_4 periods were 11, -72, 16, and 39 W m^{-2}, respectively.

The minute fluctuations in T_{svc} described in section 5b (2) are caused by abrupt changes in Q_{net} (from positive to negative and vice versa) associated with the thermal effects of the vehicle.

b. Evaluation of thermal effects of vehicles

Figure 15 shows a schematic view of the heat balance in the vehicle-passage area (left) and that in the non-vehicle-passage area (right). The contribution of heat flux (R_{ld}, R_{lu}, R_s, C_p, R_v, and S) to ΔT_{sc} was quantitatively evaluated as IP* by the following equation:

$$\mathrm{IP}^* = \frac{P^*}{|R^*_{1d}| + |R^*_{1u}| + |R^*_s| + |C^*_p| + |R^*_v| + |S^*|} \quad \text{and} \tag{20}$$

$$P^* = \int_t [P_{-v}(t) - P_{-n}(t)]\, dt, \tag{21}$$

where P_{-v} is the heat flux in the vehicle-passage area (R_{ld-v}, R_{lu-v}, R_{s-v}, C_{p-v}, R_{v-v}, and S_{-v}) and P_{-n} is the heat flux in the non-vehicle-passage area (R_{ld-n}, R_{lu-n}, R_{s-n}, C_{p-n}, and S_{-n}). Note that P^* is the hourly heat flux calculated by the time integration of the subtraction of P_{-n} from P_{-v}. Thus, IP* is the rate of each P^* with regard to the sum of the absolute values of P^*. A positive IP* increases ΔT_{sc} and a negative IP* reduces ΔT_{sc}.

Next, let us consider IP* at the free-running and traffic-signal locations based on Figs. 16a and 16b, which show the time variations in IP* for cases BS and CS, respectively.

1) FREE-RUNNING LOCATION

At the free-running location, IR^*_v and IR^*_{lu} were always positive, but IR^*_{ld} and IR^*_s were always negative because of the vehicle's shielding effect. In addition, IS* was positive at 1300, 1400, and 1600 LT. This was because $T_{svc} < T_{snc}$ and V_{nw} was large. Conversely, IC^*_p IR^*_v was positive until 1200 LT and negative at 1300, 1400, and 1600 LT. This was due to the increase in C_{p-n} associated with a drop in T_{snc}.

The values of $\overline{\mathrm{IR}^*_{ld}}$, $\overline{\mathrm{IR}^*_{lu}}$, $\overline{\mathrm{IR}^*_s}$, $\overline{\mathrm{IC}^*_p}$, $\overline{\mathrm{IR}^*_v}$, and $\overline{\mathrm{IS}^*}$, which are the means of IP* over the analysis period, were -0.15, 0.10, -0.14, 0.17, 0.18, and -0.16, respectively.

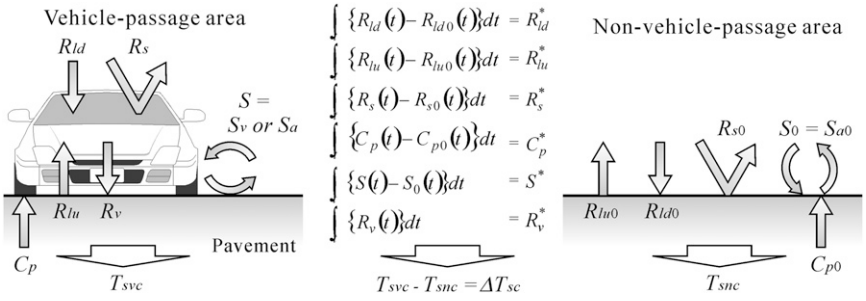

FIG. 15. Schematic view of heat balance in (left) vehicle-passage and (right) non-vehicle-passage areas.

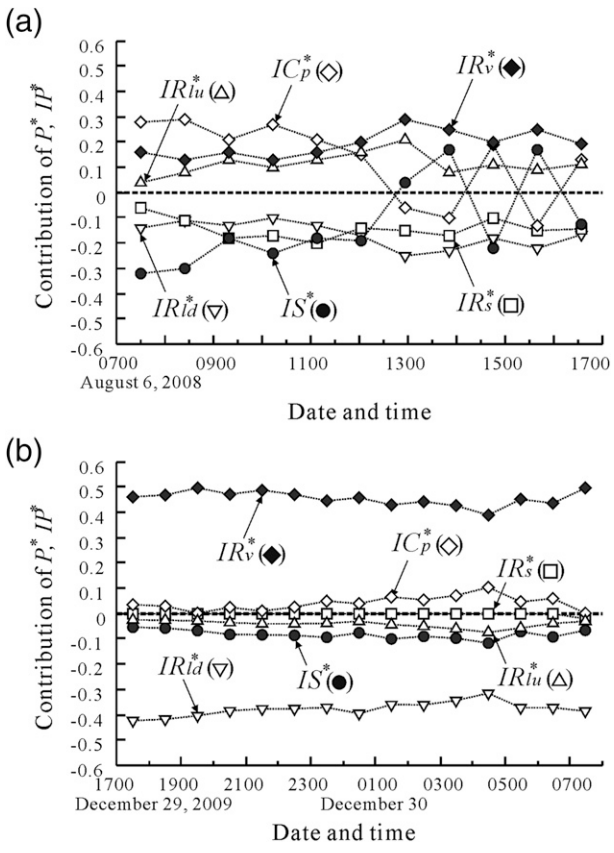

FIG. 16. Time variations in IP*: (a) free-running and (b) traffic-signal locations.

At the free-running location, it was difficult to identify the dominant heat flux that affects ΔT_{sc}.

2) TRAFFIC-SIGNAL LOCATION

At the traffic-signal location, IR^*_v and IR^*_{ld} played an important role in IP* and the contributions of IR^*_{lu}, IS*, and IC^*_p to T_{sc} were relatively small. However, the absolute values of IR^*_{lu}, IS*, and IC^*_p increased slightly toward 0400 LT, when F_v reached its minimum. Because of this increase, IR^*_v and IR^*_{ld} decreased, but they were approximately 3 times larger than the absolute values of IR^*_{lu} or IS*. At 0400 LT, the values of IR^*_{lu}, IS*, and IC^*_p were −0.07, 0.12, and −0.10, respectively.

The values of $\overline{IR^*_{ld}}$, $\overline{IR^*_{lu}}$, $\overline{IR^*_s}$, $\overline{IC^*_p}$, $\overline{IR^*_v}$, and $\overline{IS^*}$ were −0.38, −0.04, 0.00, 0.04, −0.08, and 0.46, respectively. At the traffic-signal location, R_v and R_{ld} are the main heat fluxes that affect ΔT_{sc}. However, the effects of R_{lu}, S, and C_p on ΔT_{sc} are nonnegligible when F_v becomes small.

7. Conclusions

We measured the distribution of the vehicle-induced wind velocity in the transversal direction of roads, and used a video camera to statistically evaluate the characteristics of vehicle stopping time and position at traffic-signal locations. Using these results, we developed a heat-balance road surface temperature model that considers the thermal effects of vehicles. The measured road surface temperatures were compared with the temperatures calculated by the proposed model at a free-running (single path) location and a traffic-signal location. This clarified the thermal effects of vehicles on the road surface temperature.

Our results are as follow:

1) The maximum value of the vehicle-induced wind velocity appeared at the center of the vehicle and decreased toward the roadside, following a Gaussian distribution.
2) The ratio of the vehicle-stopping period to the red-light period increased with an increase in traffic volume, following a power function. For example, this ratio was 0.25 for a traffic frequency of 50 vehicles per hour and 0.87 for 360 vehicles per hour.
3) The ratio of the number of vehicles stopping at the designated point (just before the stop line) to the total number of stopping vehicles decreased from 0.90 to 0.50 following a power function, as the traffic volume decreased.
4) For both the free-running and traffic-signal locations, the calculated road surface temperatures in the vehicle-passage area and the non-vehicle-passage area were in agreement with the observed values.
5) The computation revealed the following two points: (i) the vehicle passage at the traffic-signal location causes fluctuations in road surface temperature with a small amplitude—the road surface temperature drops during the green-light period and increases during the red-light period, and (ii) the amplitude of the fluctuations in the road surface temperature tends to increase slightly as the traffic volume increases.
6) At the free-running location, it was difficult to identify the dominant heat flux that influenced the difference in the road surface temperature between the vehicle-passage area and the non-vehicle-passage area. At the traffic-signal location, the vehicle relative heat flux and sky relative heat flux were the main contributors to this difference.

Although traffic and weather conditions were limited, the proposed model enabled the calculation of the time variation in the road surface temperature in the vehicle-passage area and direct comparison with the observed one. Consequently, it was found that the thermal contribution of vehicles to road surface temperature cannot be neglected and is significantly different between the free-running location and the traffic-signal location.

However, further studies will be needed to find the limitations of the parameterizations and formulation of the vehicle-related heat fluxes in this study through the change in vehicle size and vehicle speed.

Acknowledgments. This work was supported by KAKENHI (90456434).

APPENDIX

List of Symbols

a, b, c	Coefficients regarding V_{w0}
C_p	Pavement conductive heat flux (W m^{-2})
c_p	Specific heat of the pavement surface (kJ kg^{-1} K^{-1})
F_v	Hourly traffic volume (vehicles per hour)
$f(t), g(t)$	Unit step functions (0 or 1) to express the spikelike changes in heat flux in response to the passing of vehicles
IP*	Rate of each P^* with regard to the sum of the absolute values of P^*
$\overline{\text{IP*}}$	Mean values of IP* over the analysis period
L	Latent heat flux (W m^{-2})
L_v	Vehicle length (m)
m, c	Suffixes expressed as the measured and calculated values
N_s	Frequency of the red signal when a vehicle stops at the designated point in N_{s0}
N_{s0}	Frequency of the red signal per unit time
P_{sa}	Stopping-vehicle-number ratio ($=N_s/N_{s0}$)
P_{st}	Stop-time ratio ($=t_{40}/t_{red}$)
P_{-n}	Heat flux in the non-vehicle-passage area (R_{ld-n}, R_{lu-n}, R_{s-n}, C_{p-n}, and S_{-n})
P_{-v}	Heat flux in the vehicle-passage area (R_{ld-v}, R_{lu-v}, R_{s-v}, C_{p-v}, R_{v-v}, and S_{-v})
P^*	Hourly heat flux calculated by the time integration of the subtraction of P_{-n} from P_{-v}
Q_{net}	Net heat flux (W m^{-2})
R_{ld}	Sky radiative heat flux (W m^{-2})
R_{lu}	Road surface radiative heat flux (W m^{-2})
R_s	Shortwave (insolation) heat flux (W m^{-2})
R_v	Vehicle radiative heat flux (W m^{-2})
RH_a	Relative humidity (%)
S	Sensible heat flux (W m^{-2})
S_a	Natural wind sensible heat flux arising from V_{nw} (W m^{-2})
S_v	Vehicle-induced sensible heat flux arising from V_w (W m^{-2})
T_a	Air temperature (°C)
T_p	Temperature of the pavement surface layer (°C)
T_s	Road surface temperature (°C)
T'_{svc}	Calculated road surface temperature without vehicle-induced sensible heat (°C)
t	Time (s)
t_0	Duration of the vehicle-induced wind (s)
t_1	Period during which the road surface is covered by a moving vehicle (the vehicle-passage time) (s)
t_2	Subsequent period during which it is not covered (the non-vehicle-passage time) (s)
t_3	Vehicle deceleration time (s)
t_4	Stop time at the designated point (s)
t_{40}	Stop time corresponding to the red-signal period (s)
t_{grn}	Green-light period (s)
t_{max}	Time for the wind velocity to reach V_{wmax} from the ambient velocity (s)
t_{red}	Red-signal period (s)
V_{nw}	Natural (background) wind velocity (m s^{-1})
V_v	Vehicle speed (km h^{-1})
V_w	Vehicle-induced wind velocity (m s^{-1})
$\overline{V_w}$	Representative value of V_w (m s^{-1})
V_{wmax}	Maximum value of V_w, (m s^{-1})
V_{wmax0}	V_{wmax} at $y^* = 0$ (m s^{-1})
V^*_{wmax}	Normalized V_{wmax}
$\overline{V^*_{wmax}}$	Average of V^*_{wmax} over half of the vehicle width
V_{w0}	V_w at $y^* = 0$ (m s^{-1})
v, n	Suffixes expressed as the vehicle- and non-vehicle-passage areas
W_v	Vehicle width (m)
y	Transversal direction of the road (m)
y^*	Normalized distance
α	Albedo
ρ_p	Density of the pavement surface layer (kg m^{-3})
ΔT_s	$T_{sv} - T_{sn}$
ΔT_{svc}	Amplitude for T_{svc}
Δz_s	Thickness of the pavement surface layer (m)
$\overline{\Delta T_s}$	The average ΔT_s during the observation period

REFERENCES

Chapman, L., J. E. Thornes, and A. V. Bradley, 2001: Modeling of road surface temperatures from a geographical parameter database. Part 1. *Stat. Meteor. Appl.,* **8,** 409–419.

Crevier, L.-P., and Y. Delage, 2001: METRo: A new model for road-condition forecasting in Canada. *J. Appl. Meteor.,* **40,** 2026–2037.

Fujimoto, A., H. Watanabe, and T. Fukuhara, 2008: Effects of vehicle heat on road surface temperature of dry condition. *Proc. 14th Standing Int. Road Weather Conf.,* Standing International Road Weather Commission, Prague, Czech Republic, ID05. [Available online at http://www.sirwec.org/Papers/prague/5.pdf.]

——, A. Saida, T. Fukuhara, and T. Futagami, 2010: Heat transfer analysis on road surface temperature near a traffic light. *Proc. 17th ITS World Congress,* Busan, South Korea, Intelligent Transportation Society, T_AP01138.

Gustavsson, T., and J. Bogren, 1991: Infrared thermography in applied road climatological studies. *Int. J. Remote Sens.,* **19,** 1311–1328.

Ishikawa, N., H. Narita, and Y. Kajiya, 1999: Contribution of heat from traffic vehicles to snow melting on roads. *Transp. Res. Rec.,* **1672,** 28–33.

Prusa, J. M., M. Segal, B. R. Temeyer, W. A. Gallus, and E. S. Takle, 2002: Conceptual and scaling evaluation of vehicle traffic thermal effects on snow/ice-covered roads. *J. Appl. Meteor.,* **41,** 1225–1240.

Rayer, P. J., 1987: The Meteorological Office forecast road surface temperature model. *Meteor. Mag.,* **116,** 180–191.

Sass, B. H., 1992: A numerical model for prediction of road surface temperature and ice. *J. Appl. Meteor.,* **31,** 1499–1506.

Sato, T., K. Kosugi, O. Abe, S. Mochizuki, and S. Koseki, 2004: Wind and air temperature distribution in the wake of a running vehicle. *Proc. 12th Standing Int. Road Weather Conf.,* Bingen, Germany, Standing International Road Weather Commission. [Available online at http://www.sirwec.org/Papers/bingen/6.pdf.]

Shao, J., and P. J. Lister, 1996: An automated nowcasting model of road surface temperature and state for winter road maintenance. *J. Appl. Meteor.,* **35,** 1352–1361.

Surgue, J. G., J. E. Thornes, and R. D. Osborne, 1983: Thermal mapping of road surface temperatures. *Phys. Technol.,* **13,** 212–213.

Takahashi, N., R. A. Tokunaga, M. Asano, and N. Ishikawa, 2006: Developing a method to predict road surface temperatures—Applying heat balance model considering traffic volume. *Proc. 13th Standing Int. Road Weather Conf.,* Turin, Italy, Standing International Road Weather Commission, 58–66. [Available online at http://www.sirwec.org/Papers/torino/9.pdf.]

Watanabe, H., A. Fujimoto, and T. Fukuhara, 2005: Modeling of heat supply to pavement from vehicle. *Proc. 21th Cold Region Technology Conf.,* Sapporo, Japan, Amer. Soc. of Civil Engineers, 195–200.